A Control Strategy for the Stable Operation of Shunt Active Power Filters in Power Grids

Majid Mehrasa[1], Edris Pouresmaeil[2,3], Sasan Zabihi[4], Eduardo M. G. Rodrigues[2], and João P. S. Catalão[2,3,5,*]

[1] Young Researchers and Elite Club, Sari Branch, Islamic Azad University, Sari, Iran
[2] University of Beira Interior, R. Fonte do Lameiro, 6201-001 Covilhã, Portugal
[3] INESC-ID, Inst. Super. Tecn., University of Lisbon, Av. Rovisco Pais, 1, 1049-001 Lisbon, Portugal
[4] ABB Australia Pty Limited, 0828, Berrimah, Northern Territory, Australia
[5] Faculty of Engineering of the University of Porto, R. Dr. Roberto Frias, 4200-465 Porto, Portugal.

***Abstract*-This paper introduces a control strategy for the assessment of shunt active power filters (SAPF) role in the electrical power networks. The proposed control scheme is based on the Lyapunov control theory and defines a stable operating region for the interfaced converter during the integration time with the utility grid. The compensation of instantaneous variations of reference current components in the control loop of SAPF in ac-side, and dc-link voltage oscillations in dc-side of the proposed model, is thoroughly considered in the stable operation of interfaced converter, which is the main contribution of this proposal in comparison with other potential control approaches. The proposed control scheme can guarantee the injection of all harmonic components of current and reactive power of grid-connected loads, with a fast dynamic response that results in a unity power factor between the grid currents and voltages during the integration of SAPF into the power grid. An extensive simulation study is performed, assessing the effectiveness of the proposed control strategy in the utilization of SAPF in power networks.**

***Index Terms*— Shunt active power filters (SAPF); voltage source converter (VSC); harmonic current components; reactive power compensation.**

I. Nomenclature

Indices		$\sum_{n=2}^{\infty} P_{SFhn}$	SAPF active power in harmonic frequencies
s	a,b,c	P_{SF}	Active power of SAPF
j	d,q	Q_{SF}	Reactive power of SAPF
Variables		$V(x)$	Lyapunov Function
i_{SFs}	Current components of SAPF	r	Radius of HCF
v_{dc}	dc-link voltage	c	Centre of HCF
v_{gs}	Grid voltages	u^{*}_{eqj}	Reference of switching state function
i_{gs}	Grid currents	i^{*}_{SFj}	Reference current of SAPF in dq frame
i_{ls}	Load current	$\sum_{n=2}^{\infty} i^{*}_{SFjhn}$	harmonic currents injected by SAPF

* Corresponding author at the Faculty of Engineering of the University of Porto
E-mail address: catalao@ubi.pt (J.P.S. Catalão).

u_{eqj}	Switching state function of SAPF	v_s	Voltage at the PCC
i_{SFs}	Current of SAPF in dq frame	i_{dc}	dc-link current
v_m	Maximum voltage amplitude at the PCC	***Parameters***	
$\tilde{I}_{av_j}$	Average values of reference currents	R_g	Resistance of grid
I_{SFj1}	Currents of SAPF in main frequency	L_g	Inductance of grid
i_{jhx}	Load harmonic components not supplied by SAPF	R_{SF}	Resistance of SAPF
$\sum_{n=2}^{\infty} i_{ljhx}$	Harmonic current components of load	L_{SF}	Inductance of SAPF
Abbreviation		R_T	Resistance of transformer
PI	Proportional-Integral	L_T	Inductance of transformer
CCF	Capability Curve of Filter	R'_{SF}	Sum of R_{SF} and R_T
SAPF	Shunt Active Power Filter	L'_{SF}	Sum of L_{SF} and L_T
HCF	Harmonic Curve of Filter	C	Capacitor of dc link
THD	Total Harmonic Distortion	(α_i, β_i)	Constant coefficients for the dynamic state switching functions
DLC	Direct Lyapunov Control	ω	Grid angular frequency

II. Introduction

Nonlinear loads connection to the power grid causes harmonic pollution through drawing nonlinear currents from the utility grid. Circulation of these harmonic components of currents throughout the feeders and the protection elements of the network generates Joule losses and electromagnetic disseminations which can interfere with other components connected to the grid, and adversely affect the performance of control loop and protection network in the whole system [1-5]. This concept has been widely investigated as a major prohibition to achieve a pure source of energy with a high power quality meeting the standard level of harmonic distortion, and unity power factor in the main grid. To reach these goals, several structures of power filters i.e., passive [6], shunt [7-8], series [9], and combination of shunt and series active filters with passive components [10-11] have been presented as solutions in a polluted electric network. Among active filter topologies, shunt active power filter (SAPF) with its naive implementation is paid more attentions in both time and frequency domains to facilitate the compensation of harmonic currents and reactive power of non-linear loads [12]. In [13], a digital implementation of fuzzy control algorithm has been presented for the SAPF in power system. A control method is presented in [14] for the control of a three-level neutral-point-clamped converter and the injection of harmonic current components of nonlinear loads. The proposed control method can also guarantee a unity power factor for the utility grid. A control plan also presented in [15] to reject the uncertainties

from the power grid. The proposed scheme is based on the fuzzy logic control theory and guarantees a stable voltage across the dc-link of interfaced converter beside its fast dynamic response in tracking the reference current. A model reference adaptive control technique is presented in [16] for the single-phase SAPF to enhance the power factor of utility grid and drop the harmonic contaminations from the line currents. A nonlinear control technique based on feedback linearization theory is employed in [17] for the control of multilevel converter topologies utilized as interfacing systems between the renewable energy resources and the distribution grid. By utilization of this method, harmonic current components and reactive power of grid-connected loads are supplied through the integration of renewable energy resources to the grid. In [18], an adaptive linear neuron technique has been proposed as a harmonic extraction strategy for the control of SAPF in power network. The performance of this control technique in compensation of harmonic current components of nonlinear loads has been compared with the instantaneous reactive power theory. Proposed control strategy in [19] is able to generate the reference current of SAPF in a-b-c reference frame in which this reference generation process works in both the three-phase and single-phase electric systems. Two integrated predictive and adaptive controllers based on artificial neural networks (ANNs) are employed in [20] for SAPF, to perform a fast estimation of reference current components and reach the first estimate through the convergence of the adaptive ANN based network algorithm. Dynamic state behaviour of dc-link voltage is used in a predictive controller for the decline of total harmonic distortion (THD). An approach of active filter allocation in DC traction networks is proposed in [21]. The filter allocation is accomplished based on the most sensitive zones of power system in order to perform the allocation determination according to the characteristics of dynamic performance in traction load. In [22], a control algorithm based on equivalent fundamental positive-sequence voltage is proposed. The reference currents of the proposed filter is achieved through a simplified adaptive linear combiner neural network by the detection of voltage magnitude of source and phase angle at the fundamental frequency, during the presence of distorted and unbalanced voltage sources and load currents. Adaptive hysteresis bands in bipolar/unipolar forms are introduced in [23-26] for the development of a current control method for APFs in order to achieve a higher quality of reference waveform tracing, less switching losses and a lower cost of construction. A sliding-mode-based control technique is presented in [27] to enhance the ability of tracing action, and power quality, and to minimize the consumption of reactive power in both transient and steady state operating

conditions. In [28] and [29] a Lyapunov function, based on the state variables of a single phase SAPF is used to decrease the harmonic level and to improve the power quality of system during the connection of various nonlinear loads to the grid. Furthermore, a modified technique has been proposed to achieve a global stability for the interfacing system and to reject the ripple of dc-side voltage components [29]. A Direct Lyapunov control method proposed in [30] for the control of SAPF combined with series-passive filter. The proposed control technique improves the power quality of utility grid by the injection of harmonic current components during the connection of nonlinear loads to the grid. Several other potential control algorithms have been presented in previous papers and reports to enhance the power quality of the grid. In this paper, the authors are proposing a control scheme for the stable operation of SAPF during the integration into the power grid. The compensation of instantaneous variations of reference currents caused by the harmonic current components of nonlinear loads and, dc-link voltage oscillations in dc-side voltage, on the operation of interfaced converter are considered properly which is the main contribution of this work.

The rest of the paper is organized into five sections. Following the introduction, general schematic diagram of the proposed SAPF will be introduced in section III and elaborated properly in the steady state operating mode. Application of Lyapunov control theory for the control and stable operation of interfacing system during transient and steady-state operating conditions will be presented in section IV. Moreover, simulations are performed to demonstrate the efficiency and applicability of the developed control plan in section V. Eventually, some conclusions are drawn in section VI.

III. Proposed Model Analysis

Schematic diagram of the proposed SAPF model is illustrated in Fig.1. The proposed model is composed of a three phase voltage-source converter with a dc-link voltage. By using a three phase static transformer, the filter is connected into the utility grid and a three phase diode-bridge rectifier with a resistor load acts as a nonlinear load, which draws a current with harmonic components from the main grid, continuously. The proposed topology is connected in parallel to the grid, and compensates total harmonic current components during the dynamic and steady state operating conditions. In order to investigate the dynamic response of the proposed control plan, the switch, *sw1,* is utilized to integrate the SAPF into the grid, abruptly.

Figure 1

A. Analysis of Harmonic Current Compensation

The main objectives of SAPF are to produce total harmonic currents sunk by the nonlinear loads and to achieve a unit power factor for the utility grid. Dynamic equations of the proposed model developed to design an effective control scheme are as follows,

$$\begin{aligned} L'_{SF}\frac{di_{SF_d}}{dt}+R'_{SF}i_{SF_d}-\omega L'_{SF}i_{SF_q}+u_{eq_d}v_c-v_d=0\\ L'_{SF}\frac{di_{SF_q}}{dt}+R'_{SF}i_{SF_q}+\omega L'_{SF}i_{SF_d}+u_{eq_q}v_c-v_q=0\\ C\frac{dv_c}{dt}-u_{eq_d}i_{SF_d}-u_{eq_q}i_{SF_q}+i_{dc}=0 \end{aligned} \quad (1)$$

By considering the reference values of currents and voltages for steady state operating condition of model, Eq. (1) can be extended as,

$$L'_{SF}\frac{di^*_{SF_d}}{dt}+R'_{SF}i^*_{SF_d}-\omega L'_{SF}i^*_{SF_q}+u^*_{eq_d}v^*_c-v_m=0 \quad (2)$$

$$L'_{SF}\frac{di^*_{SF_q}}{dt}+R'_{SF}i^*_{SF_q}+\omega L'_{SF}i^*_{SF_d}+u^*_{eq_q}v^*_c=0 \quad (3)$$

$$u^*_{eq_d}i^*_{SF_d}+u^*_{eq_q}i^*_{SF_q}-I_{dc}=0 \quad (4)$$

According to (2) and (3), switching state functions of interfaced converter for the steady state operating condition can be obtained as,

$$u^*_{eq_d}=\frac{-R'_{SF}}{v^*_c}\left(\frac{L'_{SF}}{R'_{SF}}\frac{di^*_{SF_d}}{dt}+i^*_{SF_d}-\frac{\omega L'_{SF}}{R'_{SF}}i^*_{SF_q}-\frac{v_m}{R'_{SF}}\right) \quad (5)$$

$$u^*_{eq_q}=\frac{-R'_{SF}}{v^*_c}\left(\frac{L'_{SF}}{R'_{SF}}\frac{di^*_{SF_q}}{dt}+i^*_{SF_q}+\frac{\omega L'_{SF}}{R'_{SF}}i^*_{SF_d}\right) \quad (6)$$

By considering average values of instantaneous variations in reference current components of proposed SAPF as,

$$\frac{di^*_{SF_d}}{dt}=\tilde{I}_{av_d},\qquad \frac{di^*_{SF_q}}{dt}=\tilde{I}_{av_q} \quad (7)$$

and substituting equations (5)-(7) in (4), Eq. (8) can be expressed as,

$$R'_{SF}i^{*2}_{SF_d} + R'_{SF}i^{*2}_{SF_q} + \left(\tilde{I}_{av_d}L'_{SF} - V_m\right)i^*_{SF_d} + \tilde{I}_{av_q}L'_{SF}i^*_{SF_q} + v^*_c I_{dc} = 0 \quad (8)$$

Equation (8) can be rewritten as,

$$\left(i^*_{SF_d} + \frac{\tilde{I}_{av_d}L'_{SF} - v_m}{2R'_{SF}}\right)^2 + \left(i^*_{SF_q} + \frac{L'_{SF}\tilde{I}_{av_q}}{2R'_{SF}}\right)^2 = \frac{\left(\tilde{I}_{av_d}L'_{SF} - v_m\right)^2 + \tilde{I}^2_{av_q}L'^2_{SF} - 4R'_{SF}v^*_c I_{dc}}{4R'^2_{SF}} \quad (9)$$

Equation (9) can be plotted as indicated in Fig. 2. As can be seen from this figure, the injected current components from the SAPF to the grid should be located inside a circle which is based on the reference current components, with a centre of $\left(-\frac{\tilde{I}_{av_d}L'_{SF} - v_m}{2R'_{SF}}, -\frac{L'_{SF}\tilde{I}_{av_q}}{2R'_{SF}}\right)$ and a radius of $\sqrt{\frac{\left(\tilde{I}_{av_d}L'_{SF} - v_m\right)^2 + \tilde{I}^2_{av_q}L'^2_{SF} - 4R'_{SF}v^*_c I_{dc}}{4R'^2_{SF}}}$.

Figure 2

For the compensation of harmonic current components of loads, reference current components in the control loop of SAPF should be defined as,

$$i^*_{SF_d} = I_{SFd_1} + \sum_{n=2}^{\infty} i^*_{SF_{d_{hn}}} \quad (10)$$

$$i^*_{SF_q} = I_{SFq_1} + \sum_{n=2}^{\infty} i^*_{SF_{q_{hn}}} \quad (11)$$

Based on the objectives of SAPF, the q-components of current in control loop of SAPF should be defined based on q-component of load current at both the main and harmonic frequencies, to reach a unity value for the power factor of utility grid. Furthermore, d-component of load current in the fundamental frequency should be sourced by the grid; consequently $I_{SFd_1} = 0$. By substituting equations (10) and (11) in (9), Eq. 12 can be expressed as,

$$\left(\sum_{n=2}^{\infty} i^*_{SF_{d_{hn}}} + \frac{\tilde{I}_{av_d}L'_{SF} - v_m}{2R'_{SF}}\right)^2 + \left(\sum_{n=2}^{\infty} i^*_{SF_{q_{hn}}} + \frac{2R'_{SF}I_{SFq_1} + L'_{SF}\tilde{I}_{av_q}}{2R'_{SF}}\right)^2 = \frac{\left(\tilde{I}_{av_d}L'_{SF} - v_m\right)^2 + \tilde{I}^2_{av_q}L'^2_{SF} - 4R'_{SF}v^*_c I_{dc}}{4R'^2_{SF}} \quad (12)$$

Equation (11) is the equation of a circle with the centre of $c=\left(-\frac{\tilde{I}_{av_d}L_{SF}^{'}-v_m}{2R_{SF}^{'}},-\frac{2R_{SF}^{'}I_{SFq_1}+L_{SF}^{'}\tilde{I}_{av_q}}{2R_{SF}^{'}}\right)$ and the radius of $r=\sqrt{\frac{\left(\tilde{I}_{av_d}L_{SF}^{'}-v_m\right)^2+\tilde{I}_{av_q}^2L_{SF}^{'2}-4R_{SF}^{'}v_c^*I_{dc}}{4R_{SF}^{'2}}}$ as illustrated in Fig.3. This circle demonstrates the capacity of proposed SAPF for generating d and q components of total harmonic currents, which is called as the Harmonic Curve of Filter (HCF). As evident, a typical load consumption region which is surrounded by the HCF, clarifies the maximum capacity of interfaced converter in the proposed SAPF at the final covering point.

Figure 3

During the operation mode, the d-axis current of SAPF should be as follows,

$$\sum_{n=2}^{\infty}i_{SF_{d_{hn}}}^{*}=\sqrt{\frac{\left(\tilde{I}_{av_d}L_{SF}^{'}-v_m\right)^2+\tilde{I}_{av_q}^2L_{SF}^{'2}-4R_{SF}^{'}v_c^*I_{dc}}{4R_{SF}^{'2}}-\left(i_{l_q}+\frac{L_{SF}^{'}\tilde{I}_{av_q}}{2R_{SF}^{'}}\right)^2}-\left(\frac{\tilde{I}_{av_d}L_{SF}^{'}-v_m}{2R_{SF}^{'}}\right) \tag{13}$$

Moreover, the d and q components of load current in harmonic frequencies are defined as,

$$\sum_{n=2}^{\infty}i_{l_{d_{hn}}}=\sum_{n=2}^{\infty}i_{SF_{d_{hn}}}^{*}+i_{d_{hx}} \tag{14}$$

$$\sum_{n=2}^{\infty}i_{l_{q_{hn}}}=\sum_{n=2}^{\infty}i_{SF_{q_{hn}}}^{*}+i_{q_{hx}} \tag{15}$$

where $i_{d_{hx}}$ and $i_{q_{hx}}$ are fundamental components of loads which are not supplied through the SAPF. According to (12), (14), and (15), Eq. (16) can be calculated as,

$$\left(\sum_{n=2}^{\infty}i_{l_{d_{hn}}}+\frac{\tilde{I}_{av_d}L_{SF}^{'}-2R_{SF}^{'}i_{d_{hx}}-v_m}{2R_{SF}^{'}}\right)^2+\left(\sum_{n=2}^{\infty}i_{l_{q_{hn}}}+\frac{2R_{SF}^{'}I_{SFq_1}+L_{SF}^{'}\tilde{I}_{av_q}-2R_{SF}^{'}i_{q_{hx}}}{2R_{SF}^{'}}\right)^2 \tag{16}$$
$$=\frac{\left(\tilde{I}_{av_d}L_{SF}^{'}-v_m\right)^2+\tilde{I}_{av_q}^2L_{SF}^{'2}-4R_{SF}^{'}v_c^*I_{dc}}{4R_{SF}^{'2}}$$

Equation (16) clarifies the harmonic consumption area for the load and is called the harmonic curve of load (HCL). Figure 4 shows the sequential process of approaching the HCF in order to increase the possibility of compensating for the harmonic current components of loads.

Figure 4

It is clear that the operation of SAPF can be even more effective for the load, if $i_{d_{hx}} \to 0$ and $i_{q_{hx}} \to 0$. Furthermore, d and q components of load current in the main frequency should be supplied via the main grid and SAPF respectively then, $I_{SFq_1} \to I_{lq_1}$ and $I_{gd_1} \to I_{ld_1}$.

B. Reactive Power Compensation Analysis

By considering $I_{out_{SF}} = i_{SF_d} + ji_{SF_q}$, $V_{out_{SF}} = v_d + jv_q$ and S_{SF} as the output current, voltage, and power of SAPF respectively, Eq. (17) can be expressed as,

$$S_{SF} = V^*_{out_{SF}} I_{out_{SF}} = P_{SF} + jQ_{SF} \tag{17}$$

By applying the stable operating conditions to the Eq. (17), active and reactive power of SAPF can be achieved as,

$$P_{SF} = v_m i^*_{SF_d} \tag{18}$$

$$Q_{SF} = -v_m i^*_{SF_q} \tag{19}$$

By substituting (18) and (19) in (9), Eq. (20) can be obtained as,

$$\left(P_{SF} + \frac{\tilde{I}_{av_d} v_m L'_{SF} - v_m^2}{2R'_{SF}}\right)^2 + \left(Q_{SF} - \frac{L'_{SF} v_m \tilde{I}_{av_q}}{2R'_{SF}}\right)^2 = \frac{\left(\tilde{I}_{av_d} L'_{SF} - v_m\right)^2 + \tilde{I}^2_{av_q} L'^2_{SF} - 4R'_{SF} v_c^* I_{dc}}{4R'^2_{SF}} . v_m^2 \tag{20}$$

The proposed SAPF should generate the total reactive power of load and total harmonic components of active power; therefore,

$$\left(\sum_{n=2}^{\infty} P_{SF_{hn}} + \frac{\tilde{I}_{av_d} v_m L'_{SF} - v_m^2}{2R'_{SF}}\right)^2 + \left(Q_{SF} - \frac{L'_{SF} v_m \tilde{I}_{av_q}}{2R'_{SF}}\right)^2 = \frac{\left(\tilde{I}_{av_d} L'_{SF} - v_m\right)^2 + \tilde{I}^2_{av_q} L'^2_{SF} - 4R'_{SF} v_c^* I_{dc}}{4R'^2_{SF}} . v_m^2 \tag{21}$$

where $\sum_{n=2}^{\infty} P_{SF_{hn}}$ is the total harmonic frequencies of active power, injected through the SAPF. Equation (21) is drawn in Fig. 5, which is called as capability curve of the filter (CCF). CCF shows the maximum capability of SAPF for injection of harmonic current components and achieving a unit power factor in the utility grid. The maximum area of a load which can be supplied by the CCF is demonstrated in Fig. 5 and is limited as the final covering point.

Figure 5

IV. Dynamic State Analysis of the Proposed Model

Sudden interconnections of SAPF into the power grid and load increment or decrement leads to some distortions in the control loop of SAPF. Proposed control scheme should be designed to track the unpredictable changes and to enable the variables of controller to follow the reference values, precisely. To reach a stable control model with a fast dynamic response during the presence of dynamic changes in the parameters of network is the main aim of this section.

A. Direct Lyapunov Control (DLC) Method

If the state variables of SAPF are kept out from their desired values, the system will be shifted into an unstable region. DLC method maintains the system in asymptotic stability area with each initial condition which is called as global asymptotical stability and helps the state variables to reach their equilibrium points during the presence of large disturbances, with a fast transient response. A system with total energy function of V(x) would be considered as a stable system, if it meets the following conditions,

$$\begin{cases} V(0)=0 \\ V(x)>0 \quad \forall x\neq 0 \\ V(x)\to\infty \ as \ \|x\|\to\infty \\ \dfrac{dV(x)}{dt}<0 \quad \forall x\neq 0 \end{cases} \tag{22}$$

By defining the error variables of SAPF as $x_1 = i_{SF_d} - i^*_{SF_d}$, $x_2 = i_{SF_q} - i^*_{SF_q}$ and $x_3 = v_c - v^*_c$, V(x) can be expressed as,

$$V(x)=\frac{1}{2}L'_{SF}x_1^2+\frac{1}{2}L'_{SF}x_2^2+\frac{1}{2}Cx_3^2 \tag{23}$$

The switching functions of interfaced converter in SAPF are defined as,

$$u_{eq_d}=u^*_{eq_d}+U_{eq_d} \tag{24}$$

$$u_{eq_q}=u^*_{eq_q}+U_{eq_q} \tag{25}$$

where $U_{eq_i}\ (i=d,q)$ are dynamic parts of the switching state functions in the interfaced converter. Considering the conditions given in (22),

$$\frac{dV(x)}{dt}=L'_{SF}x_1\frac{dx_1}{dt}+L'_{SF}x_2\frac{dx_2}{dt}+Cx_3\frac{dx_3}{dt}<0 \tag{26}$$

According to (1) and substituting the defined error variables, the derivative part of (26) can be expressed as,

$$
\begin{aligned}
L_{SF}^{'}\frac{dx_1}{dt} &= -R_{SF}^{'}x_1+\omega L_{SF}^{'}x_2-\frac{\left(-L_{SF}^{'}\tilde{I}_{av_d}-R_{SF}^{'}i_{SF_d}^{*}+\omega L_{SF}^{'}i_{SF_q}^{*}+e_m\right)}{v_c^{*}}x_3-U_{eq_d}v_c+e_m \\
L_{SF}^{'}\frac{dx_2}{dt} &= -R_{SF}^{'}x_2-\omega L_{SF}^{'}x_1-\frac{\left(-L_{SF}^{'}\tilde{I}_{av_q}-R_{SF}^{'}i_{SF_q}^{*}-\omega L_{SF}^{'}i_{SF_d}^{*}\right)}{v_c^{*}}x_3-U_{eq_q}v_c \\
C\frac{dx_3}{dt} &= \frac{\left(-L_{SF}^{'}\tilde{I}_{av_d}-R_{SF}^{'}i_{SF_d}^{*}+\omega L_{SF}^{'}i_{SF_q}^{*}+e_m\right)}{v_c^{*}}x_1+\frac{\left(-L_{SF}^{'}\tilde{I}_{av_q}-R_c i_{SF_q}^{*}-\omega L_{SF}^{'}i_{SF_d}^{*}\right)}{v_c^{*}}x_2+U_{eq_d}i_{SF_d} \\
&+U_{eq_q}i_{SF_q}-\left(i_{dc}-I_{dc}\right)
\end{aligned}
\tag{27}
$$

By substituting (27) and defined error values each part of (26) can be obtained as,

$$
\begin{aligned}
L_{SF}^{'}x_1\frac{dx_1}{dt} &= -R_{SF}^{'}x_1^2+\omega L_{SF}^{'}x_2x_1-u_{eq_d}^{*}x_1x_3-U_{eq_d}x_1v_c+x_1e_m \\
L_{SF}^{'}x_2\frac{dx_2}{dt} &= -R_{SF}^{'}x_2^2-\omega L_{SF}^{'}x_1x_2-u_{eq_q}^{*}x_2x_3-U_{eq_q}x_2v_c \\
Cx_3\frac{dx_3}{dt} &= u_{eq_d}^{*}x_3x_1+u_{eq_q}^{*}x_3x_2+U_{eq_d}x_3i_{SF_d}+U_{eq_q}x_3i_{SF_q}-x_3\left(i_{dc}-I_{dc}\right)
\end{aligned}
\tag{28}
$$

By substituting (28) in (26), derivative of total energy in proposed model can be obtained as,

$$
\begin{aligned}
\frac{dV(x)}{dt} &= -R_{SF}^{'}\left(i_{SF_d}-i_{SF_d}^{*}\right)^2-R_{SF}^{'}\left(i_{SF_q}-i_{SF_q}^{*}\right)^2-U_{eq_d}\left(v_c^{*}i_{SF_d}-v_c i_{SF_d}^{*}\right)-U_{eq_q}\left(v_c^{*}i_{SF_q}-v_c i_{SF_q}^{*}\right) \\
&-\left(i_{dc}-I_{dc}\right)\left(v_c-v_c^{*}\right)
\end{aligned}
\tag{29}
$$

According to Eq. (29), dynamic part of the switching state functions in the proposed SAPF can be achieved as,

$$U_{eq_d}=\alpha\left(v_c^{*}i_{SF_d}-v_c i_{SF_d}^{*}\right) \tag{30}$$

$$U_{eq_q}=\beta\left(v_c^{*}i_{SF_q}-v_c i_{SF_q}^{*}\right) \tag{31}$$

Equations (29) and (30) are used for the stabilization of closed loop control during the dynamic changes. dc-voltage fluctuations lead to interference in the performance of DLC method and operation of SAPF. In order to eliminate these interferences and their negative impacts, value of v_c should tend to the value of v_c^{*}.

B. Impacts of α and β in DLC method

The constant and positive coefficients of α and β are considered as important factors for regulating the operation of SAPF to reach a unity power factor in the utility grid and improve the THD of grid currents with a fast transient response during the load changes and sudden integration of SAPF into the main grid. In order to investigate the impacts of α and β in the performance of DLC method, dynamic model of SAPF should be analysed during the presence of error in variables of the proposed model,

$$L_{SF}^{'}\frac{dx_1}{dt}+R_{SF}^{'}x_1-\omega L_{SF}^{'}x_2+u_{eq_d}^{*}x_3+U_{eq_d}v_c-\left(v_d-v_m\right)=0 \tag{32}$$

$$L_{SF}^{'}\frac{dx_2}{dt}+R_{SF}^{'}x_2+\omega L_{SF}^{'}x_1+u_{eq_q}^{*}x_3+U_{eq_q}v_c-v_q=0 \tag{33}$$

$$C\frac{dx_3}{dt}-u_{eq_d}^{*}x_1-u_{eq_q}^{*}x_2-U_{eq_d}i_{SF_d}-U_{eq_q}i_{SF_q}+\left(i_{dc}-I_{dc}\right)=0 \tag{34}$$

With respect to the dynamic part of switching state functions of interfaced converter, equations (32)-(34) can be linearized around an operating points as,

$$\begin{aligned}
\frac{dx_1}{dt}&=\left(\frac{-R_{SF}^{'}-\alpha v_c^{*2}}{L_{SF}^{'}}\right)x_1+\left(\omega\right)x_2+\left(\frac{\alpha i_{SF_d}^{*}v_c^{*}-u_{eq_d}^{*}}{L_{SF}^{'}}\right)x_3+\frac{\left(v_d-v_m\right)}{L_{SF}^{'}}\\
\frac{dx_2}{dt}&=-\left(\omega\right)x_1+\left(\frac{-R_{SF}^{'}-\beta v_c^{*2}}{L_{SF}^{'}}\right)x_2+\left(\frac{\beta i_{SF_q}^{*}v_c^{*}-u_{eq_q}^{*}}{L_{SF}^{'}}\right)x_3+\frac{v_q}{L_{SF}^{'}}\\
\frac{dx_3}{dt}&=\left(\frac{\alpha v_c^{*}i_{SF_d}^{*}+u_{eq_d}^{*}}{C}\right)x_1+\left(\frac{\beta v_c^{*}i_{SF_q}^{*}+u_{eq_q}^{*}}{C}\right)x_2-\left(\frac{\alpha i_{SF_d}^{*2}+\beta i_{SF_q}^{*2}}{C}\right)x_3+\left(\frac{I_{dc}-i_{dc}}{C}\right)
\end{aligned} \tag{35}$$

The state matrix of SAPF in both dynamic and steady state operating conditions can be obtained as,

$$A=\begin{bmatrix}
\frac{-R_{SF}^{'}-\alpha v_c^{*2}}{L_{SF}^{'}} & \omega & \frac{\alpha i_{SF_d}^{*}v_c^{*}-u_{eq_d}^{*}}{L_{SF}^{'}}\\
-\omega & \frac{-R_{SF}^{'}-\beta v_c^{*2}}{L_{SF}^{'}} & \frac{\beta i_{SF_q}^{*}v_c^{*}-u_{eq_q}^{*}}{L_{SF}^{'}}\\
\frac{\alpha v_c^{*}i_{SF_d}^{*}+u_{eq_d}^{*}}{C} & \frac{\beta v_c^{*}i_{SF_q}^{*}+u_{eq_q}^{*}}{C} & -\frac{\alpha i_{SF_d}^{*2}+\beta i_{SF_q}^{*2}}{C}
\end{bmatrix} \tag{36}$$

All inherent frequencies of the proposed model can be achieved by solving matrix A. Apparently, the natural frequencies of the proposed SAPF state variables are highly dependent on α and β; therefore, the stable region of the model is enhanced by a proper selection of these coefficients. Figure 6 shows the impact of dynamic gains variation on the THD of grid current in phase "a". As can be seen, while the coefficients are increased, the value of THD is noticeably decreased and remains in a constant value around 0.6 % for the last three coefficient values. Power factor between the grid current and the voltage of phase "a" and also transient time responses during the sudden connection of SAPF are changed by the variations in dynamic gains, according to Table 1. Table 1 clarifies that, the PF is improved while the coefficients are increased and power factor of the grid reaches the unity value for the gains more than 1e-5. On the other hand, the transient time significantly reduced by increasing the values of dynamic gains.

Figure 6

Table 1

V. Results and Discussions

The proposed model in Fig.1 is simulated through Matlab/Simulink platform, to validate the performance of DLC technique in a SAPF application. General schematic diagram of SAPF including DLC structure is depicted in Fig. 7. The simulation parameters are given in Table 2. A three phase diode rectifier with a 30Ω resistive load has been considered as a nonlinear load which is connected to the main grid and draws a nonlinear current continuously from the utility grid. In order to evaluate the dynamic and the steady-state responses of DLC technique and harmonic current compensation of nonlinear load, SAPF is connected to the grid through the $sw1$.

Figure 7

Table 2

A. Interconnection of SAPF to the utility grid

In this section, the capability of DLC method is evaluated during the connection of SAPF into the grid and the presence of nonlinear loads. Before connection of SAPF to the grid, a nonlinear load is connected to the grid and draws harmonic current components from the utility source. This

process is continued until t=0.1 sec, where SAPF is connected to the grid through the sw1. Figure 8 indicates the load, grid, and SAPF currents before and after integration of SAPF into the power grid. As can be seen, before the integration of SAPF into the grid, all components of the load current are injected through the grid, but after the connection of SAPF to the grid, supplied current by the utility grid to the load is sinusoidal and free of harmonic components; then, all the harmonic components of the load current are supplied through the SAPF.

Figure 8

The capability of DLC technique in following the reference current components in the control loop of SAPF is demonstrated in Fig. 9. As shown in this figure, after the connection of SAPF to the grid, all the harmonic parts of d-component in the load current are generated through the SAPF which confirms that the grid only generates the d-component of the load current at the main frequency. In addition, when SAPF is connected to the grid, both harmonic and main frequencies of the load current in q-axis are supplied through the SAPF; therefore, the injected current from grid to the load is free of q-component.

Figure 9

B. Active and reactive power sharing

Active and reactive power generation through the SAPF is another objective of the DLC technique. Figure 10 shows the active power sharing between the SAPF, the load, and the grid. As apparent in this figure, total harmonic portion of the load active power is injected via the SAPF and utility grid only sources constant active power of 7.5 kW which is in the fundamental frequency.

Figure 10

Figure 11 shows the reactive power sharing between the SAPF, the load, and the main grid. According to this figure, after the connection of SAPF, total reactive power of load is entirely supplied through the SAPF and the reactive power provided by the grid is reduced to the zero. This figure confirms the capability of DLC method to compensate the load reactive power and the application of SAPF as a power factor correction device.

Figure 11

C. THD and Power Factor Analysis

Achieving unity power factor for the grid and reaching a low THD for the current injected from the grid, are the two main objectives of DLC technique in the proposed SAPF control scheme. Figure 12 shows the grid voltage and current at phase “a”. As indicated in this figure, after the connection of SAPF into the grid, grid current is sinusoidal and in phase with the load voltage. Therefore, the drawn current from the grid is free of harmonic current components and also reactive power components; then, a unity power factor is achieved immediately after connection of SAPF. Figure 13 depicts the power factor between the voltage and the current of the grid in phase (a), before and after the connection of SAPF to the grid. As can be seen, after the connection of SAPF, power factor of utility grid reaches the unity value. Power factor values in three phases of utility grid are presented in table 3, before and after the connection of SAPF to the utility grid.

Figure 12

Figure 13

Table 3

Figure 14 shows the THD of the load and the grid currents during the connection of SAPF into the grid. This confirms an appropriate performance of DLC technique in decreasing the harmonic current components of the grid current during the presence of nonlinear loads. THDs of the grid currents are given in table 4, before and after the connection of SAPF which demonstrates the performance of DLC method in compensation of harmonic current components of nonlinear loads.

Figure 14

Table 4

VI. Conclusion

The paper has presented and analysed the utilization of shunt active power filter (SAPF) in power grids. A control scheme based on the Lyapunov control theory has been proposed for the grid connection and the stable operation of SAPF during its integration with utility grid. General model

of the proposed plan was developed in dynamic and steady state operating conditions and impacts of different parameters on the stable operation of interfaced converter has been properly considered. An extensive simulation analysis has been carried out, evaluating the performance of the proposed control plan for the compensation of nonlinearity caused through the connection of nonlinear loads to the main grid. In all the durations, simulation results confirmed the injection of harmonic current components and reactive power of nonlinear loads from SAPF. By this assumption, the injected current from the grid to the nonlinear load achieved sinusoidal shape and was free of any reactive power and harmonic current components; then, the power factor between the grid current and voltage reached a unity value. The proposed control strategy can be used for the integration of renewable energy resources as power quality enhancement device in a custom power distribution network during the presence of industrial loads.

VII. Acknowledgements

João Catalão and Edris Pouresmaeil thank the EU Seventh Framework Programme FP7/2007–2013 under grant agreement no. 309048, FEDER through COMPETE and FCT, under FCOMP-01-0124-FEDER-020282 (Ref. PTDC/EEA-EEL/118519/2010), UID/CEC/50021/2013 and SFRH/BPD/102744/2014.

References

[1] Mehrasa M, Pouresmaeil E, Akorede MF, Jørgensen BN, Catalão JPS. Multilevel converter control approach of active power filter for harmonics elimination in electric grids. Energy 2015; 84: 722-731.

[2] Xiu-xing Yin, Yong-gang Lin, Wei Li, Ya-jing Gu, Hong-wei Liu, Peng-fei Lei. A novel fuzzy integral sliding mode current control strategy for maximizing wind power extraction and eliminating voltage harmonics. Energy 2015; 85: 677-686.

[3] Personal E, Guerrero JI, Garcia A, Peña M, Leon C. Key performance indicators: A useful tool to assess Smart Grid goals. Energy 2014; 76: 976-988.

[4] Rekik M, Abdelkafi A, Krichen L. a micro-grid ensuring multi-objective control strategy of a power electrical system for quality improvement. Energy 2015; 88: 351–363.

[5] Melício R, Mendesc VMF, Catalão JPS. Comparative study of power converter topologies and control strategies for the harmonic performance of variable-speed wind turbine generator systems. Energy 2011; 36(1): 520–529.

[6] Barote L, Marinescu C. Software method for harmonic content evaluation of grid connected converters from distributed power generation systems. Energy 2014; 66: 401-412.

[7] Derafshian M, Amjady N. Optimal design of power system stabilizer for power systems including doubly fed induction generator wind turbines. Energy 2015; 84: 1-14.
[8] Pouresmaeil E, Mehrasa M, Shokridehaki M.A, Shafie-khah M, Rodrigues E.M.G, Catalao J.P.S. Stable Operation of Grid-Interfacing Converter during the Operation of Active Power Filters in Power Grids. Compatibility and Power Electronics (CPE), 2015 9th International Conference on, 132 - 137.
[9] Senturk O S, Hava A M. Performance Enhancement of the Single-Phase Series Active Filter by Employing the Load Voltage Waveform Reconstruction and Line Current Sampling Delay Reduction Methods. IEEE Transactions on Power Electronic 2011; 26(8): 2210–2220.
[10] Caramia P, Carpinelli G, Gagliardi F, Verde P. Analysis and design of a combined system of shunt passive and active filters. European Transactions on Electrical Power 1994; 4(2): 155–162.
[11] Litran S P, Salmeron P. Analysis and design of different control strategies of hybrid active power filter based on the state model. IET Power Electron 2012; 5(8): 1341–1350.
[12] Sonnenschein M, Weinhold M. Comparison of time-domain and frequency-domain control schemes for shunt active filters. European Transactions on Electrical Power 1999; 9(1): 5–16.
[13] Singh B N, Singh B, Chandra A, Al-Haddad K. Digital implementation of fuzzy control algorithm for shunt active filter. European Transactions on Electrical Power 2000; 10(6): 369–375.
[14] Pouresmaeil E., Montesinos-Miracle, D., Gomis-Bellmunt, O., and Sudria-Andreu, A. “Instantaneous Active and Reactive Current Control Technique of Shunt Active Power Filter Based on the Three-Level NPC Inverter,” European Trans on Electric Power 2011; 21(7): 2007–2022.
[15] Mikkili S, Panda A K. Performance analysis and real-time implementation of shunt active filter Id-Iq control strategy with type-1 and type-2 FLC triangular M.F. International Transactions on Electrical Energy Systems Article, DOI: 10.1002/etep.1698.
[16] Shyu K, Yang M J, Chen Y M, Lin Y F. Model Reference Adaptive Control Design for a Shunt Active-Power-Filter System. IEEE Transactions on Industrial Electronics, 2008; 55(1): 97–106.
[17] Pouresmaeil E, Gomis-Bellmunt O, Montesinos-Miracle D, Bergas-Jané J. Multilevel converters control for renewable energy integration to the power grid. Energy 2011; 36(2): 950–963.
[18] Vardar K, Akpinar E “Comparing ADALINE and IRPT methods based on shunt active power filters,” European Transactions on Electrical Power2011; 21(1): 924–936.
[19] Ramos-Carranza H A, Medina1 A, Chang G W “Real-time application of shunt active power filter dynamic compensation using real-time windows target,” International Transactions on Electrical Energy Systems2013; 23(8): 1289–1303.
[20] Bhattacharya A, Chakraborty C, “A shunt active power filter with enhanced performance using ANN-based predictive and adaptive controllers” IEEE Trans. Ind. Electron.2011; 58(2): 421–428,
[21] Cantor E L, Ramos G A, Ríos M A, Albarracín A .Allocation of active power filter in DC traction systems. International Transactions on Electrical Energy Systems2013; 23(7): 1191–1204.

[22] Chang G W, Hong R C, Su H J. An efficient reference compensation current strategy of three-phase shunt active power filter implemented with processor-in-the-loop simulation. International Transactions on Electrical Energy Systems2014; 24(1): 125–140.

[23] Zabihi, Sasan and Zare, Firuz. ; “A New Adaptive Hysteresis Current Control with Unipolar PWM Used in Active Power Filters” [online]. Australian Journal of Electrical & Electronics Engineering, Vol. 4, No. 1, 2008: 9-16.

[24] Zabihi, S.; Zare, F.; "Active Power Filters with Unipolar Pulse Width Modulation to Reduce Switching Losses," Power System Technology, 2006. PowerCon 2006. International Conference on , vol., no., pp.1-5, 22-26 Oct. 2006

[25] Zare, F.; Zabihi, S.; Ledwich, G.; "An adaptive hysteresis current control for a multilevel inverter used in an active power filter," Power Electronics and Applications, 2007 European Conference on , vol., no., pp.1-8, 2-5 Sept. 2007

[26] Zabihi, Sasan; Zare, Firuz; “An Adaptive Hysteresis Current Control Based on Unipolar PWM for Active Power Filters,” *Proceedings of the 2006 Australasian Universities Power Engineering Conference*, 10-13 December 2006, Australia, Victoria, Melbourne.

[27] Ghamria A, Benchouiaa M T, Goleaa A. Sliding-mode Control Based Three-phase Shunt Active Power Filter: Simulation and Experimentation. Electric Power Components and Systems.2012; 40(4): 383–398.

[28] Hua C, Li C-H, Lee C-S, “Control analysis of an active power filter using Lyapunov candidate,” IET Power Electron 2008; 2(4):325–334.

[29] Komurcugil, H., Kukrer, O. A new control strategy for single-phase shunt active power filters using a Lyapunov function. IEEE Trans. Ind. Electron 2006; 53(1):305–312.

[30] Rahmani S, Hamadi A, Al-Haddad K. A Lyapunov-Function-Based Control for a Three-Phase Shunt Hybrid Active Filter. IEEE Trans. Ind. Electron 2012; 59(3): 1418–1429.

Figure captions

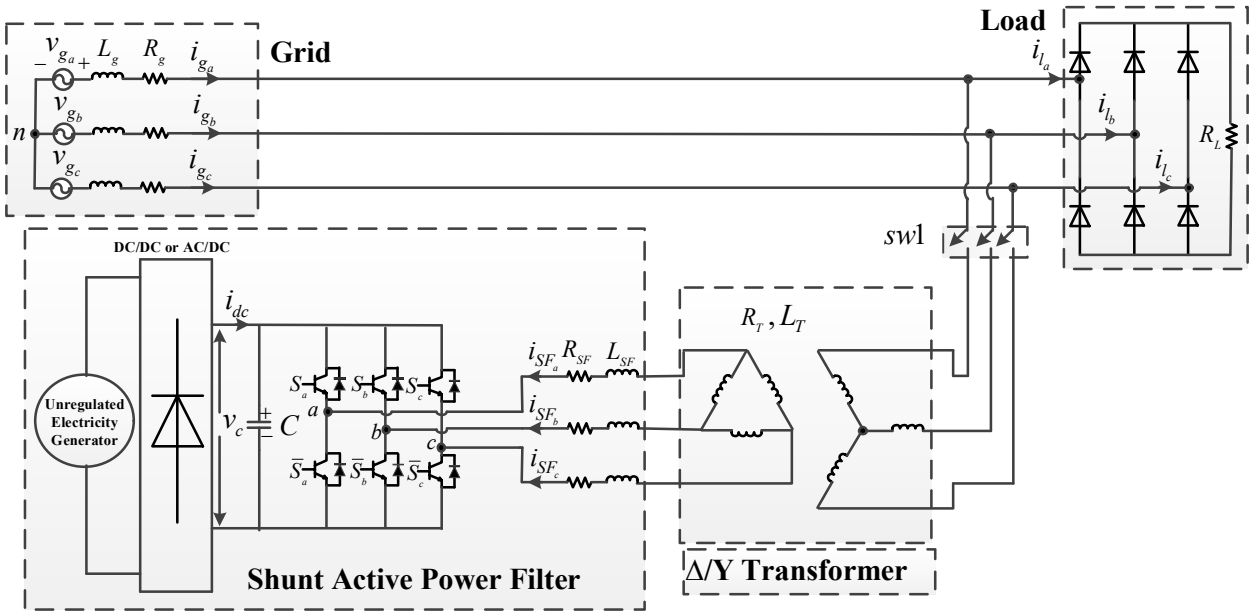

Fig.1. Schematic diagram of the proposed SAPF model.

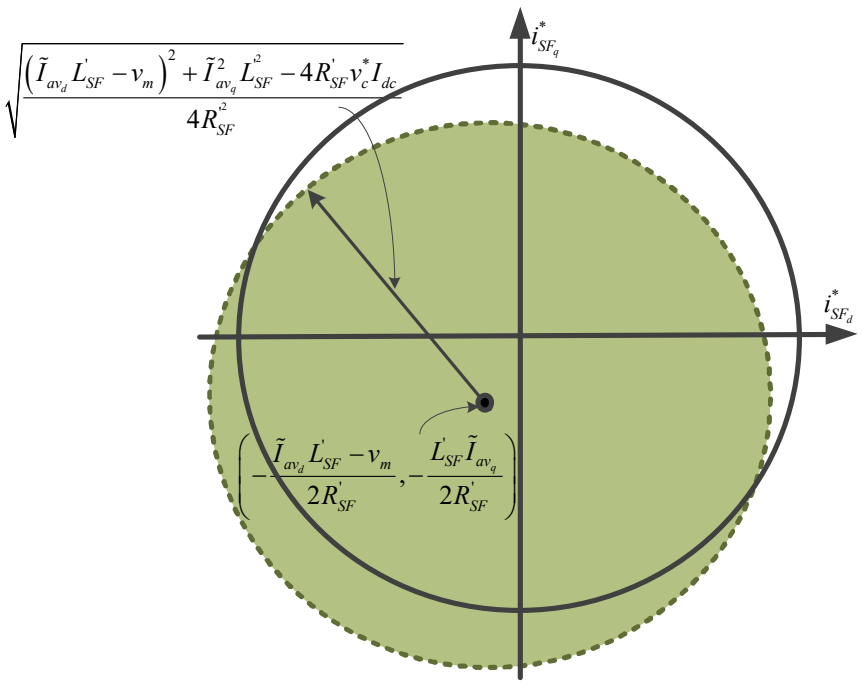

Fig. 2. $i^*_{SF_q}$ versus $i^*_{SF_d}$ of SAPF in steady state operating condition.

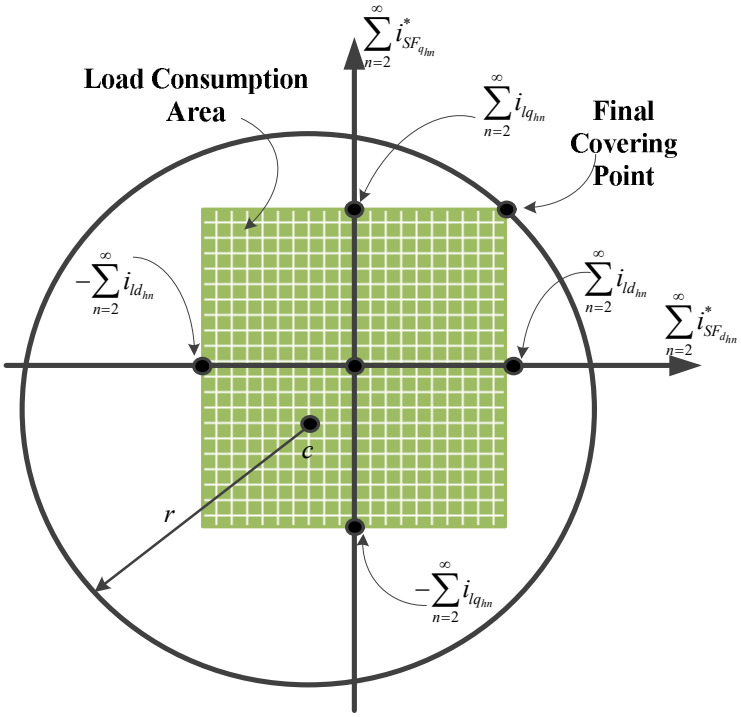

Fig. 3. Harmonic Curve of SAPF.

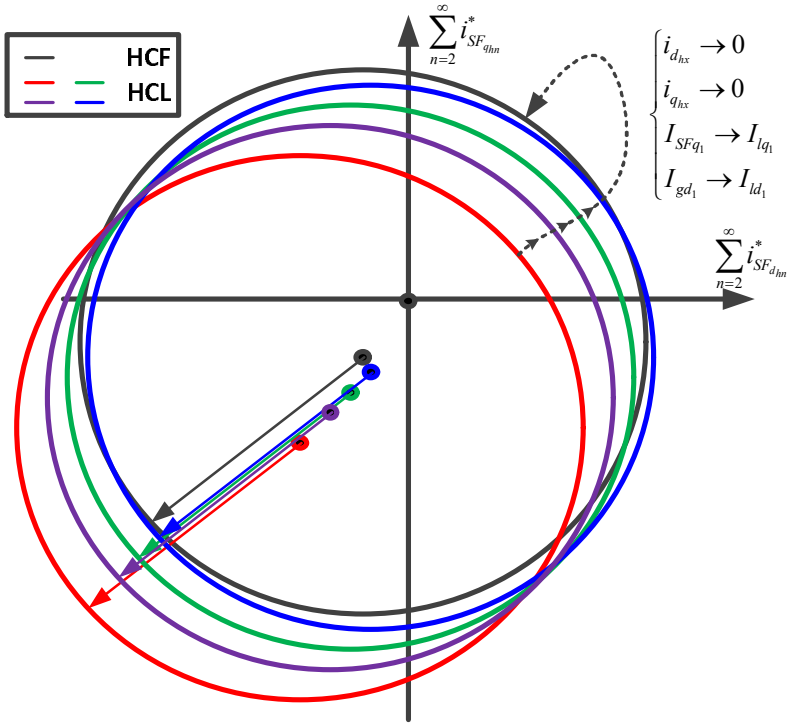

Fig. 4. Harmonic Curve of SAPF.

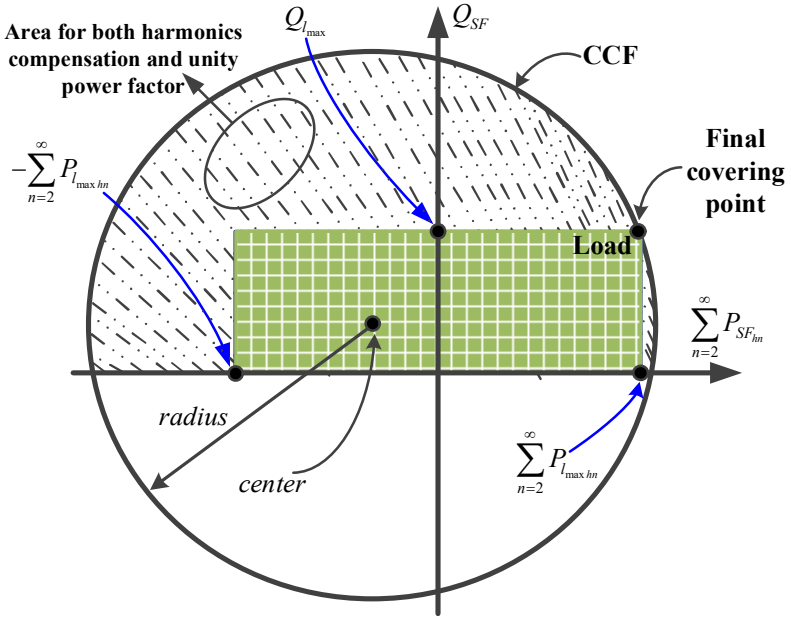

Fig. 5. Capability Curve of SAPF.

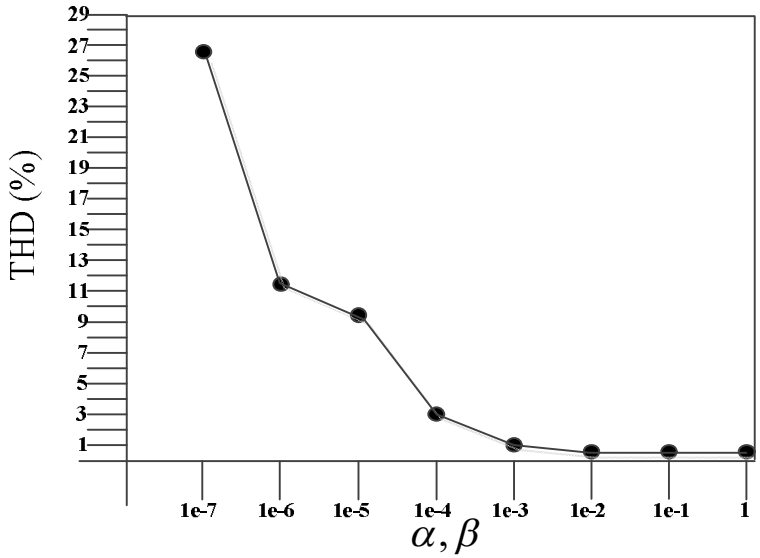

Fig.6. Impacts of variations of dynamic gains on THD of grid current.

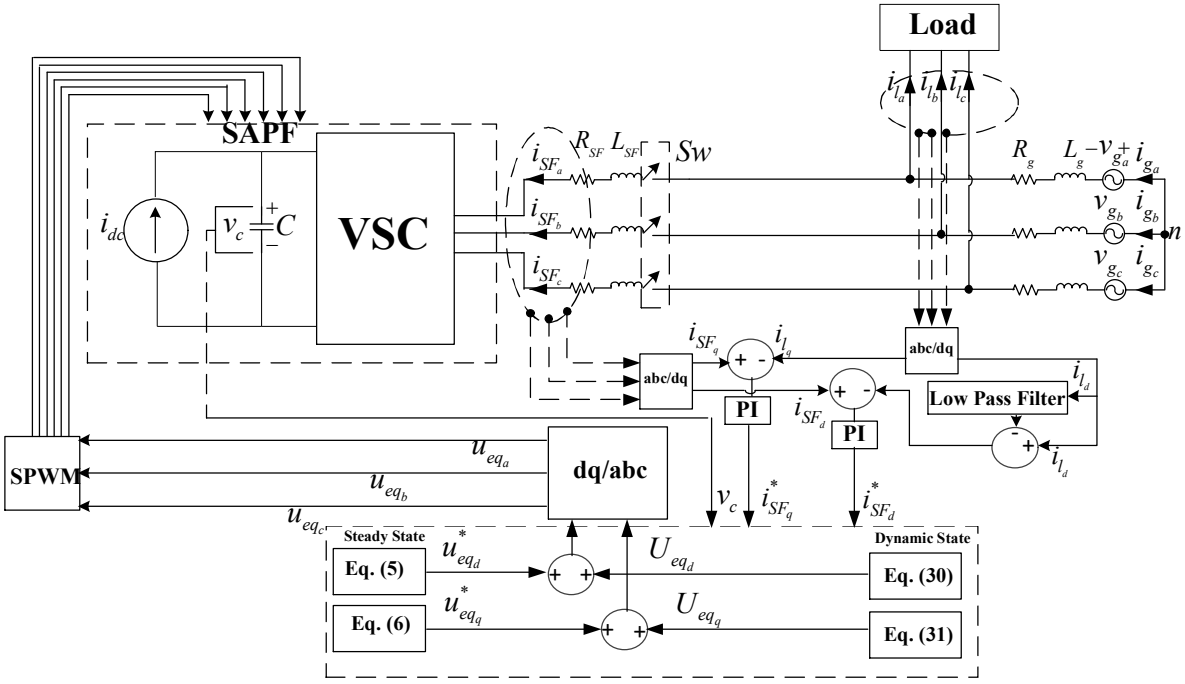

Fig.7. Schematic diagram of SAPF and DLC method.

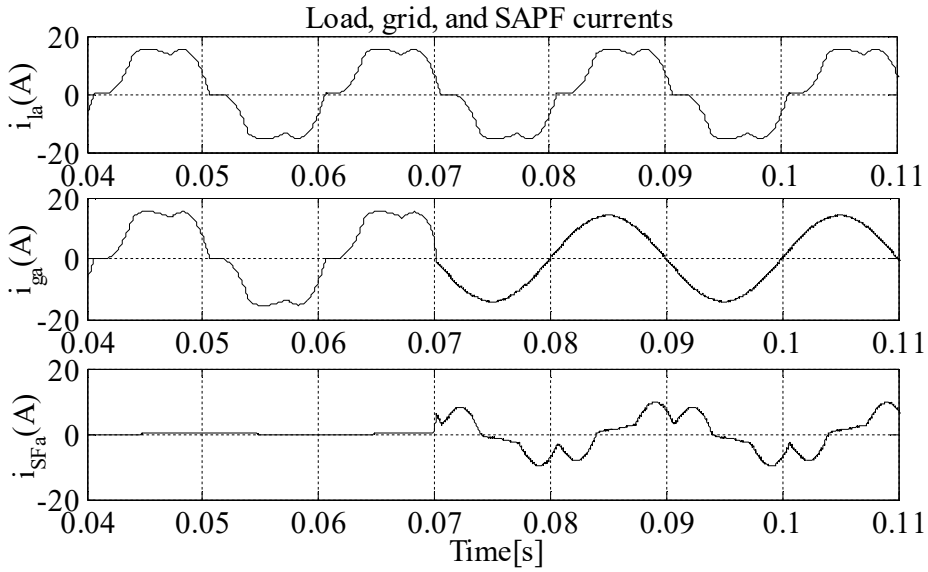

Fig.8. Load, grid, and SAPF currents, before and after connection of SAPF to the power grid.

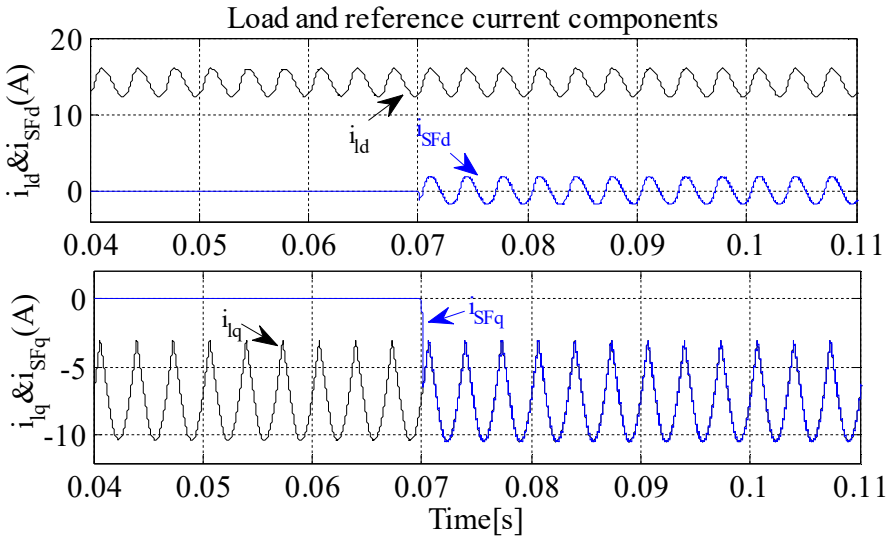

Fig.9. d and q components of load and SAPF currents, before and after connection of SAPF to the grid.

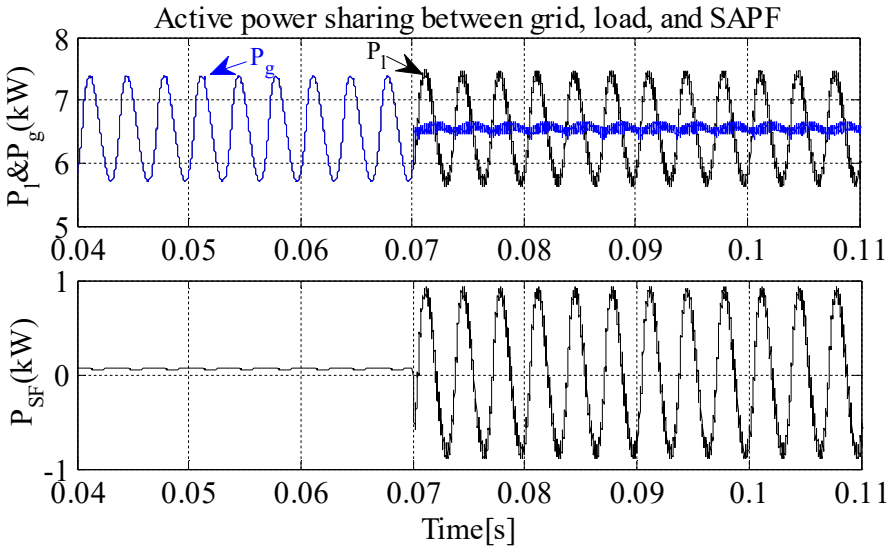

Fig.10. Active power sharing between the load, grid, and SAPF before and after connection of SAPF to the grid.

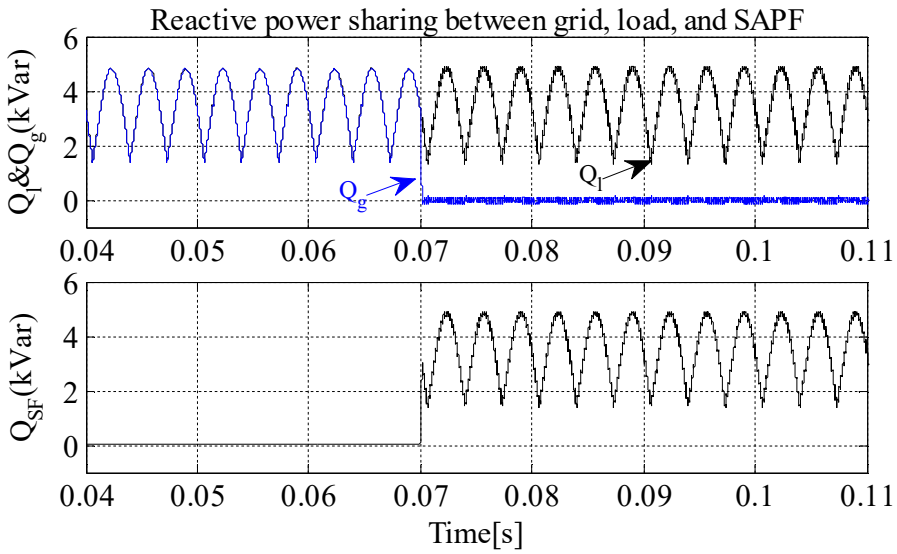

Fig.11. Reactive power sharing between the load, grid, and SAPF before and after connection of SAPF.

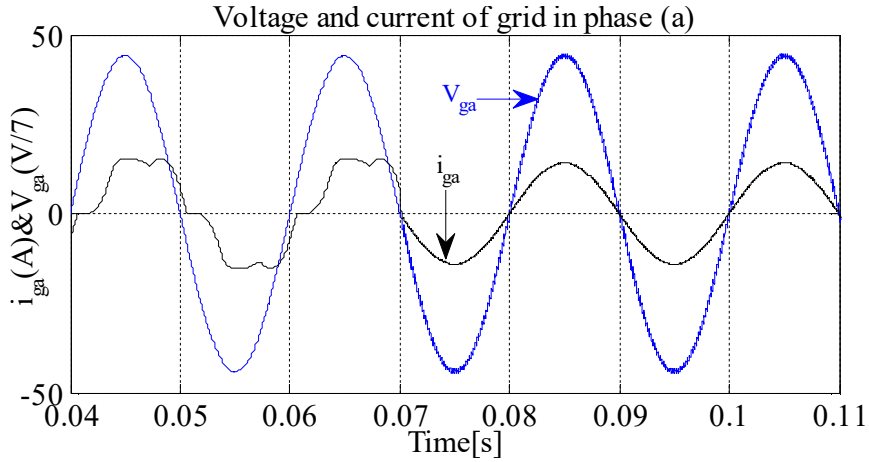

Fig.12. Grid voltage and current in phase (a), before and after connection of SAPF to the grid.

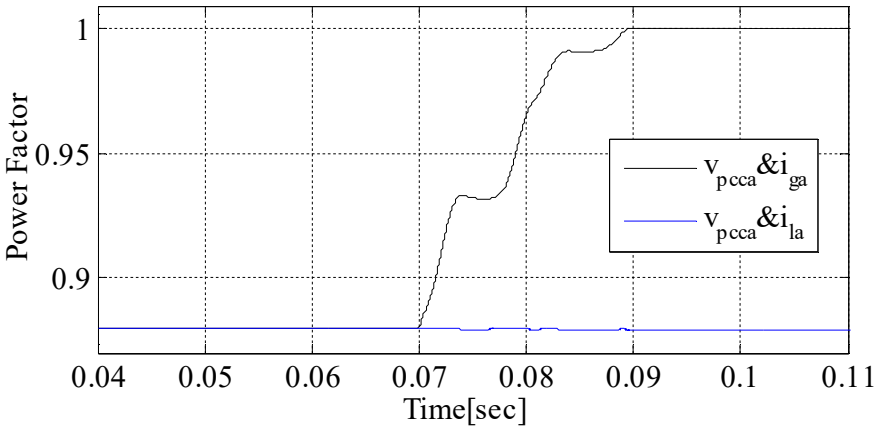

Fig.13. Power Factor between the load voltage and grid current in phase (a) before and after connection of SAPF to the grid.

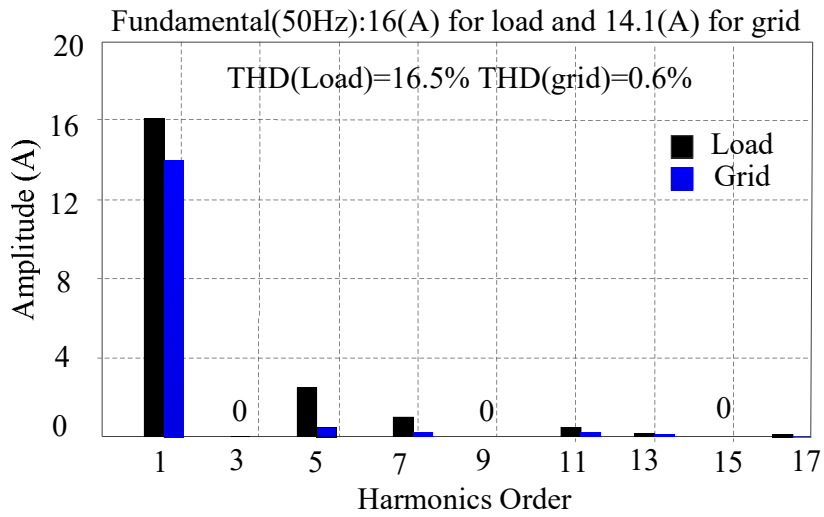

Fig.14. THD of load and grid currents at phase (a) after connection of SAPF to the grid.

Tables

Table 1. Impacts of variations of dynamic gains on power factor and Transient Responses.

α, β	1e-7	1e-6	1e-5	1e-4	1e-3	1e-2	1e-1	1
Power Factor (%)	50.31	77.1	99.06	100	100	100	100	100
Transient Response (ms)	eps	80	60	30	20	20	20	20

Table 2. Simulation parameters.

Grid Voltage	380 rms V
Input Voltage	1000 volt DC
Main Frequency	50 Hz
Inverter Resistance	0.1 Ω
Inverter Inductance	0.45 mH
α	0.01
β	0.001
Switching Frequency	10 kHz
SAPF Power Rating	19 kVA

Table 3. Power Factor analysis.

PF Grid	Before Connection	After Connection
PF1 (%)	88.5	100
PF2 (%)	88.4	100
PF3 (%)	88.6	100

Table 4. THD of grid currents.

Grid Currents	Before Connection	After Connection
i_{ga} (%)	16.6	0.6
i_{gb} (%)	16.51	0.61
i_{gc} (%)	16.42	0.62